

## Analysis of the Heterogeneity of pO<sub>2</sub> Dynamics During Photodynamic Therapy with Verteporfin<sup>¶</sup>

Brian W. Pogue\*<sup>1</sup>, Rod D. Braun<sup>2</sup>, Jennifer L. Lanzen<sup>2</sup>, Christian Erickson<sup>2</sup> and Mark W. Dewhirst<sup>2</sup>

<sup>1</sup>Thayer School of Engineering, Dartmouth College, Hanover, NH and

<sup>2</sup>Department of Radiation Oncology, Duke University Medical Center, Durham, NC

Received 5 March 2001; accepted 21 August 2001

### ABSTRACT

Photodynamic therapy (PDT) with verteporfin provides a reliable way to destroy malignant tissues. Changes in the blood flow and oxygen partial pressure (pO<sub>2</sub>) during verteporfin-PDT were studied here in the tumor tissue of the rat mammary R3230Ac carcinoma model. Oxygen microelectrodes (6–12 μm tip diameter) were used to measure the transients locally within tumors during intravenous injection of 1.0 mg/kg verteporfin followed by irradiation 15 min later with 690 nm light at 200 mW/cm<sup>2</sup>, for a cumulative dose of 144 J/cm<sup>2</sup>. The observed changes in pO<sub>2</sub> were heterogeneous and there was a difference in the response of low-pO<sub>2</sub> regions relative to higher-pO<sub>2</sub> regions. The change in pO<sub>2</sub> in hypoxic tissue regions (pO<sub>2</sub> < 8 mmHg) had acute pO<sub>2</sub> loss after treatment, whereas the response in regions of higher pO<sub>2</sub> (>8 mm Hg) was more heterogeneous with some areas maintaining their pO<sub>2</sub> value after treatment was completed. Blood flow measurements taken on a subset of the animals indicated a significant loss in flow during the initial light delivery that remained low after treatment, indicating some vascular stasis. The results suggest that hypoxic or poorly perfused vessels may be more susceptible to acute stasis than normoxic vessels in this treatment protocol.

### INTRODUCTION

Photodynamic therapy (PDT) is a treatment for neoplastic and abnormal tissues that uses a combination of photosensitizer drug together with moderate-intensity light to cause selective necrosis and apoptosis of cells, as well as vascular damage (1). This therapy has recently been approved by the Food and Drug Administration for treatment of a few disease sites, and a particularly promising application is the treatment of age-related macular degeneration (2–5). The com-

bination of the commercial photosensitizer verteporfin, a lipid encapsulated preparation of benzoporphyrin derivative (BPD), together with high irradiance of light at 690 nm can have a measurable therapeutic effect in the wet form of this retinal disease (4). Basic rodent tissue studies on blood flow changes during and after treatment with verteporfin have shown that there is a specific set of dosimetric conditions that lead to vascular occlusion (6). Still the vascular shut-down process is likely heterogeneous, and the response throughout bulk tissue cannot be universally described by a single set of dosimetry conditions because variations in vessel size, flow rate and distribution within a neovascularized tissue will result in a heterogeneous response. In this study we examine how the heterogeneity of tissue oxygenation may have an impact on the success of verteporfin-PDT, with a particular emphasis on how the acute vascular occlusion efficacy is affected by the initial oxygen partial pressure (pO<sub>2</sub>).

These concerns about heterogeneity have been studied more thoroughly with regard to the use of PDT for treating tumor tissues where oxygen distribution has large microregional variations. Part of the heterogeneity is related to variations in the vascular pO<sub>2</sub>, as well as chaotic architecture and variable flow through vessels (7–13). Low vascular pO<sub>2</sub> can result from the chaotic architecture leading to longitudinal pO<sub>2</sub> gradients (*i.e.* loss of oxygen from the vessel when traversing from the arteriolar source [14]) and from low red cell flux in some microvessels (12). In this study pO<sub>2</sub> and blood flow responses were measured within the rat mammary carcinoma R3230Ac as a model for the clinical application of verteporfin-PDT in a dysplastic tissue. It is important to understand the oxygen dynamics within tissue during treatment, because this is the most direct photochemical monitor of how dose is being deposited to the tissue. However, interpretation of these dynamics is not trivial because of the mixture of photochemical and biological changes that occur during treatment. Tromberg *et al.* (15) used large polarographic electrodes to examine the rapid photochemical consumption of oxygen caused by Photofrin-PDT *in vivo*, and these transients were further mechanistically quantified *in vitro* with Clarke electrodes (16–18) to develop a predictive understanding of the photochemical consumption and photosensitizer bleaching phenomena. These early observations led to *in vivo* study of oxygen changes using Eppendorf electrode systems (19,20), and although the response is high-

<sup>¶</sup>Posted on the website on 27 September 2001.

\*To whom correspondence should be addressed at: Thayer School of Engineering, 8000 Cummings Hall, Dartmouth College, Hanover, NH 03755, USA. Fax: 603-646-3856; e-mail: pogue@dartmouth.edu

Abbreviations: BPD, benzoporphyrin derivative; LDF, laser Doppler flow; PDT, photodynamic therapy; pO<sub>2</sub>, oxygen partial pressure; SEM, standard error of mean.

© 2001 American Society for Photobiology 0031-8655/01 \$5.00+0.00

ly heterogeneous, there is a general appreciation that for Photofrin treatment the photochemical depletion of oxygen within tissues is present and reduces treatment efficacy at higher optical dose rates.

However, photochemical oxygen consumption is a major influence during treatment at high fluence rates, the treatment is further complicated by alterations in blood flow, which can also significantly change the tissue oxygenation. Localized observation of blood vessel stasis, occlusion or vessel dilation have all been observed with Photofrin treatment *in vivo* (21–23). Recently Fingar *et al.* (6) illustrated that with verteporfin-PDT, the vascular response had a significant correlation with the time after injection, indicating that shorter times between injection and irradiation were optimal to produce vascular stasis. They also concluded that dysplastic vessels required a lesser light dose to cause occlusion than normal tissue vessels. Extending these results further, it is important to know the relative contributions of flow *versus* oxygen supply in the vessel, because as the flow increases the available oxygen increases. Yet the ability to cause occlusion is likely reduced in a highly flowing vessel. At the same time, verteporfin treatment has a high photochemical oxygen consumption *in vivo* (24), indicating that in low-flowing vessels there could conceivably be a shortage of oxygen to cause effective photochemical occlusion. In this study we are interested in determining how the oxygenation affects vessel stasis during verteporfin treatment, and to what extent transient photochemical depletion affects this process.

Because changes in tumor oxygen consumption and supply can occur on a distance scale of hundreds of microns, any localized measure of bulk tissue oxygen may not reflect the microdynamics of oxygen transport in the tumor. Microelectrodes can be used to sample tissue volumes that are much less than the distance between capillaries and hence can provide information on how PDT treatment affects oxygen transport at the microregional level (25–27). Glass microelectrodes with 6–12  $\mu\text{m}$  tip diameter and a recessed tip design (25,26) were used to directly sample the  $\text{pO}_2$  in rat tumor tissue with simultaneous monitoring of the Doppler blood flow changes from implanted fibers. These measurements were used to assess the oxygen changes during treatment with verteporfin-PDT. The microelectrodes can provide the microregional information needed to assess how oxygen changes during PDT. Sampling different regions within a single tissue cannot be reliably achieved during the time-course of one treatment; however, by sampling multiple tumors in different rats, a representative distribution of tissue  $\text{pO}_2$  regions can be developed and the temporal changes within each of these regions followed. Through pooling of microsampled data among different rats, it is possible to survey the heterogeneity of responses observed within tumor tissue and to develop a summary of typical observations. This process has been studied here with a particular emphasis on correlation to the initial  $\text{pO}_2$  values as a prognostic indicator of vessel response.

## METHODS

**Photosensitizer.** Verteporfin<sup>®</sup> was obtained from QLT Inc. (Vancouver, Canada). It is composed of a sterile liposomal preparation of benzoporphyrin derivative monoacid ring "a." This powder was refrigerated for storage, and stock aqueous solutions of 0.3 mg/mL

liposomal BPD were prepared in sterile water within 48 h prior to injection into animals. The solutions were refrigerated between uses and maintained in the dark.

**Animal and tumor models.** All animal procedures were approved by the Duke University Animal Care and Use Committee. Fischer 344 rats weighing approximately 150 g (Charles River, Raleigh, NC) were purchased and used for tumor tissue implantation. Prior R3230Ac mammary adenocarcinoma tumors were harvested from tumor-bearing animals, and 0.1  $\text{mm}^3$  sections of these were transplanted into the animal's left lateral quadriceps muscle.

Animals had access to normal food and water levels for 2–3 weeks, when the tumor diameter had reached approximately 1 cm. At this tumor diameter the animals were used for these nonsurvival experiments.

Animals were anesthetized with sodium pentobarbital (50 mg/kg intraperitoneally) and placed in lateral recumbency on a thermostatically controlled blanket at 37°C (K Module; Baxter Healthcare Corp., Valencia, CA). The femoral artery and lateral coccygeal vein were cannulated for measurement of arterial blood pressure and intravenous infusion of photosensitizer. The tumor surface fur was shaved off and the overlying skin resected to expose the tumor surface. The thin tumor capsule was bluntly dissected from the front surface to facilitate insertion of the electrode into the tumor, and at the same time minimizing hemorrhage on the surface of the tumor.

**Oxygen electrode measurements.** Recessed oxygen microelectrodes were used to measure the  $\text{pO}_2$  within the tumor tissue at the site of PDT light delivery. The electrodes were constructed in the lab following the method of Linsenmeier and Yancey (28). The pertinent parameters and use of these electrodes have been discussed previously (25,26); however, the salient features will be mentioned here. Each electrode had a diameter between 6 and 12  $\mu\text{m}$  laterally and was beveled diagonally to facilitate insertion into the tissue. Electrodes were polarized at  $-0.7$  V, and the current measured with a microsensor (Model 1201 Chemical Microsensor, Diamond General, Ann Arbor, MI) and recorded on a computer using an automated data acquisition program (WinDaq, AT-Codas, Dataq Instruments, Akron, OH).

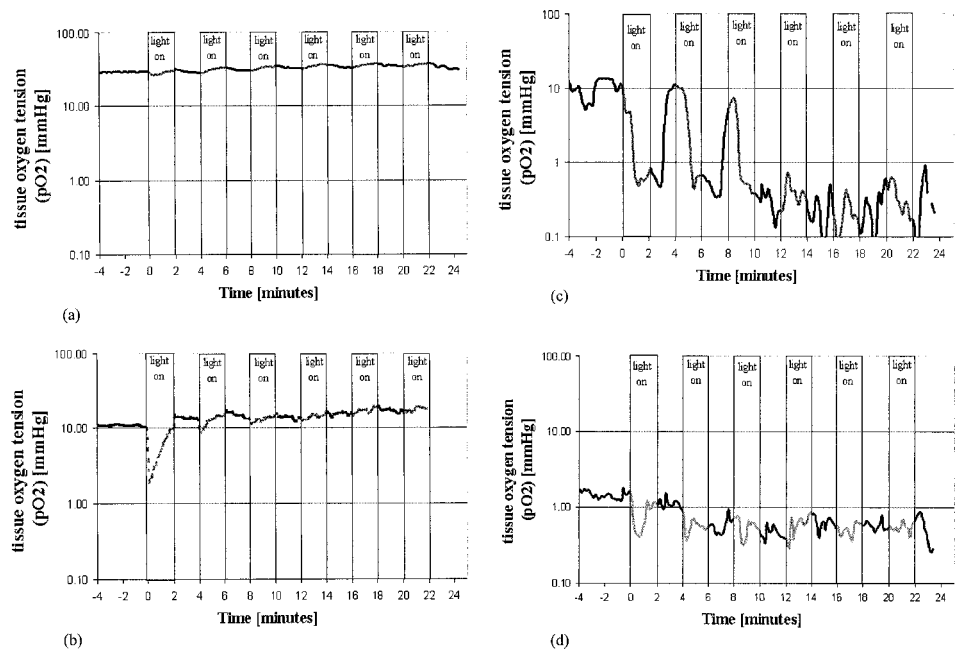
Each electrode was calibrated in saline at 37°C, which was bubbled with gas at well calibrated mixtures of 21, 15, 5 and 0% oxygen with balance nitrogen. The calibration line of  $\text{pO}_2$  *versus* current reading was determined both before and after each set of animal experiments. The *in vivo* zero  $\text{pO}_2$  calibration point for each data set was measured after euthanasia of each animal. The value was recorded after waiting for 5 min to ensure that the  $\text{pO}_2$  in the tissue had dropped to zero.

The electrode was inserted into the tumor with a micromanipulator after placing a saline drop on the exposed tumor surface. Each electrode was inserted to about 1–2 mm into the tissue and allowed to equilibrate for several minutes until a stable reading was found. The animals were placed in a Faraday cage throughout the experiment to minimize electrical interference. During the entire experiment blood pressure was recorded using computerized acquisition of femoral arterial waveforms (Gould P23XL, Gould Instrument Systems, Cleveland, OH).

**Doppler blood flow measurements.** In nine rats, laser Doppler blood flow (LDF) measurements were taken with the Oxford Array system (Oxford Optronics Ltd., Oxford, UK), using two fiber optic probes inserted into each tumor. The two fiber probes had diameters of 200  $\mu\text{m}$ , and were implanted in the tumor tissue through holes which were created with a 22 gauge needle. In most of the experiments one probe was implanted in the tumor within the light field, approximately within 2–4 mm of the oxygen electrode. The second Doppler probe was implanted in the far side of the tumor tissue, away from the light field to provide a control measure where minimal light dose was being deposited. All LDF values were expressed relative to the average value during the 2 min before the first light exposure after verteporfin injection.

**PDT treatments.** Prior to the injection of the photosensitizer, the electrode was placed in the tumor tissue, and a 2 min irradiation of light was delivered to provide a control observation of the light alone in each animal. In all cases the treatment light was delivered from a 690 nm diode laser system through a fiber optic collimator to a 1  $\text{cm}^2$  spot on the tumor tissue, for a total surface irradiance of 200  $\text{mW}/\text{cm}^2$ . The light beam was centered on the location of the oxygen

**Figure 1.** Example measurements of  $pO_2$  are shown as a function of time during the light treatments that were composed of six fractions of light (2 min each) with 2 min of light-off time between fractions. The shaded bars show the light-on time intervals, with the data lines overlapping to show the temporal transients. The graphs (a)–(d) show data from four different animal experiments.



electrode to maximize the overlap of the measurement with the treatment field. After this no-drug control measurement, the verteporfin photosensitizer stock solution was injected intravenously at a dose of 1 mg/kg in all rats 15 min prior to light irradiation. The light treatments were delivered in 2 min fractions followed by 2 min light-off fractions, to allow a visualization of the treatment effects during the irradiation. This light cycling was done for two primary reasons: (1) because the irradiation light saturated the Doppler probe so that the only useful data are between light fractions, and (2) to examine the dose–response of the vascular changes in steps of the optical dose of 24 J/cm<sup>2</sup>. The total treatment included six fractions for an incident dose of 144 J/cm<sup>2</sup>. After treatment the animals were observed for 2–5 min and then sacrificed by intravenous injection of >200 mg/kg sodium pentobarbital. After the blood pressure dropped and the  $pO_2$  stabilized near zero the probes were removed from the tumor, and the tumor was removed for pathology or photosensitizer extraction.

**Temperature measurement.** In one rat a 1 mm diameter thermistor (Mon-a-therm Model 6510, Mallinckrodt Medical, St. Louis, MO) was inserted into the tumor during irradiation to monitor the change in temperature during irradiation and to determine the level of hyperthermia involvement in this treatment protocol. An 18-gauge needle was inserted into the tumor and removed. The plastic-coated thermistor was then inserted along the needle track and positioned within the tumor. The light was positioned so that the thermistor was within the illumination field. Temperature was manually recorded from the digital readout every minute. The light was delivered in 2 or 4 min fractions while monitoring the temperature. The same rat was used to monitor the temperature increase without verteporfin and later after verteporfin injection at 1 mg/kg.

**Photosensitizer extraction.** After treatment, half the animal tumors were used for histology and half used for chemical extraction of the photosensitizer. In those tumors used for the latter assay, the tumor was resected and frozen at  $-20^{\circ}\text{C}$ , to be liquefied within 2 weeks of the treatment study. At that time, the tumors were minced and dissolved in 0.1 N NaOH solution with 2% sodium dodecyl sulfate detergent, at a total concentration of 1 mL solution per gram of tumor. These solutions were dissolved for 6 h in a  $50^{\circ}\text{C}$  water bath with constant stirring. The resulting mixtures were centrifuged at 1200 rpm for 6 min to separate out the supernatant from the remaining cellular constituents. The supernatant was poured into a 1 cm cuvette, and the fluorescence of BPD was measured in a Perkin–Elmer spectrofluorimeter, and compared with the fluorescence intensity of a set of calibrated solutions of BPD suspended in supernatant from untreated tumor tissue.

**Statistical analysis.** The absolute changes in  $pO_2$  and blood flow

during and after PDT were analyzed with a Wilcoxon signed-ranks test to determine which changes were significant.

## RESULTS

### $pO_2$ measurement

A total of 24 rats were treated with this dose of photosensitizer and light, and one additional rat was used to monitor temperature during the treatment. Two experiments were eliminated from this study because the  $pO_2$  failed to drop after euthanasia of the animal, indicating that the microelectrode was too close to the surface of the tumor and may have been influenced by oxygen at the tumor–air interface. Two experiments were excluded because the rat noticeably twitched during the experiment and the microelectrode moved within the tumor. Thus, there are reliable  $pO_2$  data from 20 rats included in this study.

Some typical traces of  $pO_2$  during the course of the treatment are shown in Fig. 1. The lines in these graphs show the  $pO_2$  as a function of time during the entire experiment on three different rat tumors. In each case, six fractions of light were given in 2 min intervals interlaced with 2 min intervals when the light was off. In all the four cases presented in Fig. 1, the  $pO_2$  decreased quite rapidly upon the initial incidence of light treatment, and in the lowest  $pO_2$  traces remained near zero after the first few light fractions. In all cases presented here, there was some recovery of the  $pO_2$  between light fractions, indicating that vascular stasis did not occur. However, there were also traces that exhibited an immediate acute decrease in  $pO_2$  that remained after the initial onset of light. In Fig. 1(b), the data set that starts at  $pO_2 = 11$  mmHg has a partial recovery during the first two light-off cycles, followed by a nonrecovery phase after that. In Fig. 1(a), starting at  $pO_2 = 29$  mmHg, the  $pO_2$  increased upon irradiation and decreased when the light was off. This pattern continued throughout the six fractions of treatment for this tumor location, and the  $pO_2$  remained high after treatment.

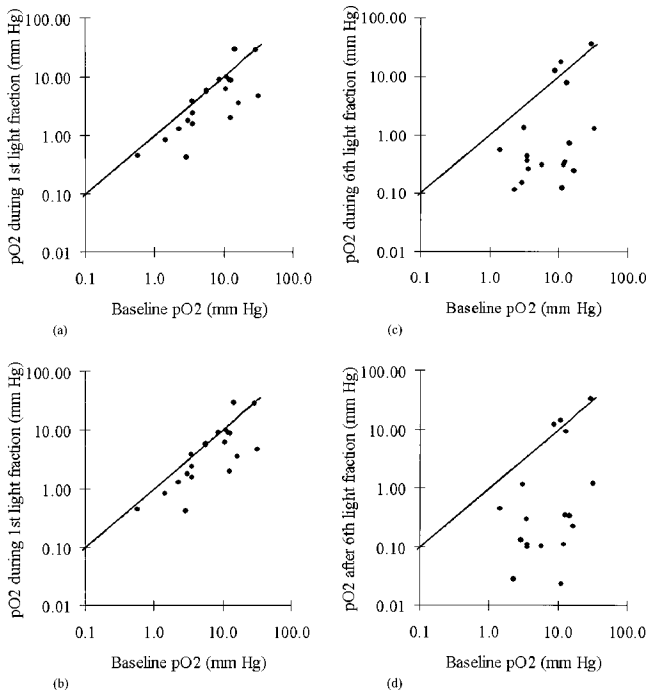


**Figure 2.** The measured average  $pO_2$  during a 2 min interval at each tumor region is plotted as a function of the initial baseline  $pO_2$  value. In (a) the  $pO_2$  values during the first light fraction are shown, (b) shows the values during the 2 min light-off period after the first fraction, (c) shows the  $pO_2$  values during the (final) sixth fraction and (d) shows the values averaged over the 2 min following completion of the light treatments. The solid lines in each figure show the line of no change in  $pO_2$  before and after treatment.

In several of the tumor locations, there were spontaneous temporal oscillations in the  $pO_2$  on the time scale of 40–60 s with about 1–2 mm Hg total magnitude, as has been documented earlier with this model system (29). In some tumors these oscillations had magnitudes varying between 5 and 10 mm Hg. In most cases these oscillations were eliminated after irradiation in those rats in whom the  $pO_2$  decreased upon irradiation. In the tumors where the  $pO_2$  did not decrease, the oscillations also remained after treatment; however, the low number of tumors exhibiting these oscillations makes it difficult to conclude precisely if these temporal changes are correlated to the observation of PDT-induced vascular occlusion.

Summary plots of all the data for the  $pO_2$  during treatment versus the initial  $pO_2$  are shown in Fig. 2. First, the data averaged during the initial 2 min light-on fraction are shown in Fig. 2(a), followed by the average data during the first light-off fraction shown in Fig. 2(b). The final  $pO_2$  during the last light fraction is shown in Fig. 2(c) and that after the entire treatment is shown in Fig. 2(d). In these data, there is an indication that  $pO_2$  regions below approximately 8 mm Hg drop to near zero values during the initial light irradiation, whereas the overall response in the  $pO_2$  regions above 8 mm Hg is less obvious. By the end of the six-fraction treatment, all the lower  $pO_2$  regions have dropped significantly, whereas above a  $pO_2$  value of 8 mm Hg there is an almost binary response to therapy where the  $pO_2$  either drops to near zero values or approximately retains its baseline value (Fig. 2[c]). In Fig. 3(a), the averaged data for all mea-

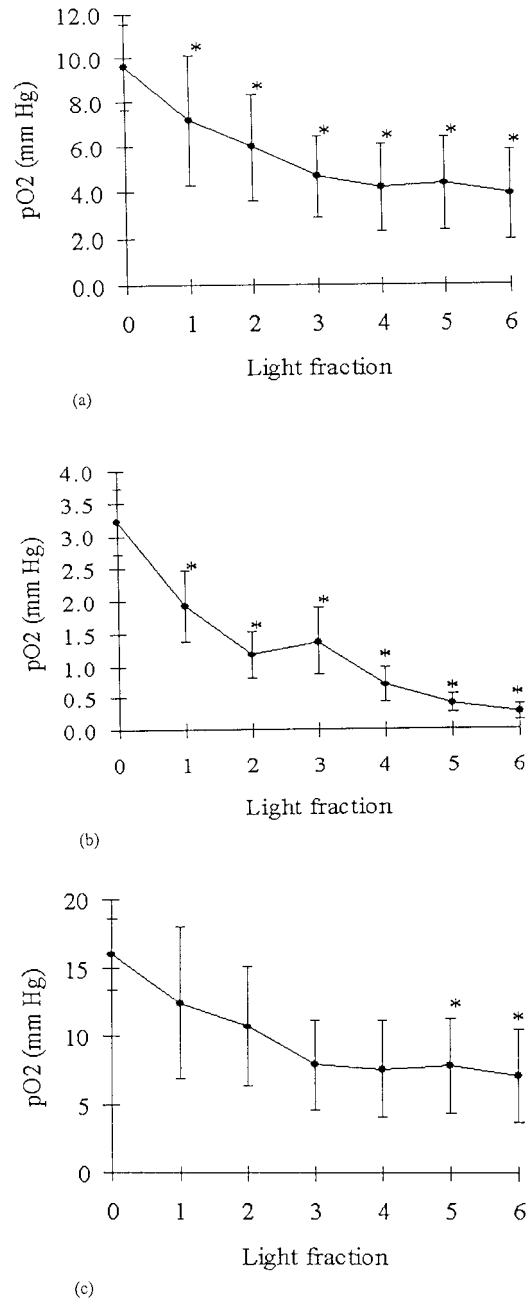


**Figure 3.** (a) Plotted mean  $pO_2$  ( $\pm$  SEM) after each light fraction are shown with the average data from all animals. The regions of  $pO_2$  (b) below and (c) above 8 mm Hg were separately averaged together to show the response in regions of initially low or high  $pO_2$ . Those data points that are significantly different from the initial baseline  $pO_2$  are indicated with an asterisk, based upon a Wilcoxon signed-ranks test.

surements are shown and there is a significant change from the initial value for all fractions ( $P < 0.02$ ). Interestingly, when the data are separated into the 10 lowest-starting  $pO_2$  values and the 10 highest-starting  $pO_2$  values (graphs shown in Fig. 3[b,c]), the changes after each fraction are significant for the regions with initial  $pO_2$  lower than 8 mm Hg shown in Fig. 3(b) ( $P < 0.004$ ), but are not significant for the regions with initial  $pO_2$  greater than 8 mm Hg (Fig. 3[c]) until the last two fractions ( $P < 0.04$ ).

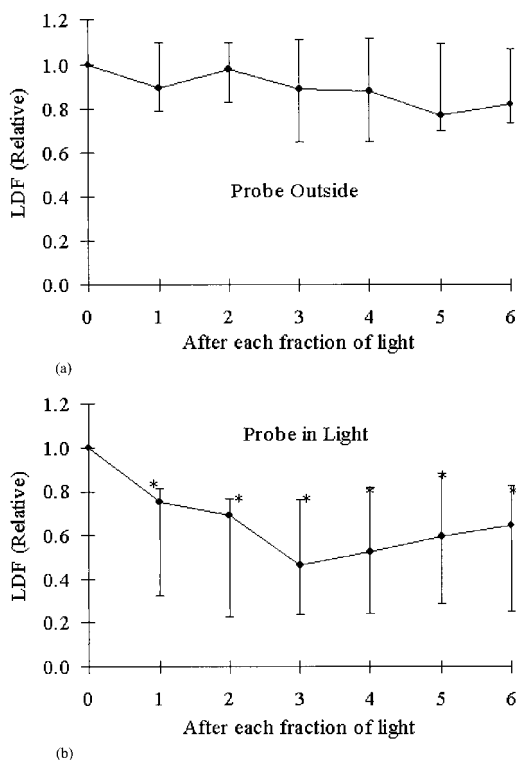


**Figure 4.** Relative laser Doppler blood flow measurements of median values are plotted as a function of the light fraction delivered to the tumor, measured both (a) exterior to the observable light field and (b) near the center of the light field. Those values that are significantly different from the initial value are marked with an asterisk, and the error bars denote the interquartile of the measurement variations.

### Laser Doppler blood flow

The Doppler blood flow measurements were affected by the light field during PDT treatment, so that during irradiation the detectors were saturated. Preliminary tests indicated the Doppler probes were only temporarily disabled by the treatment light field, and they were still able to measure accurate blood flow after being subjected to these light fields. As a result, the only meaningful comparisons of blood flow change are between the values when the treatment light was off. Using these data from the light-off fractions, changes in relative blood flow within the light field can be observed in the majority of tumors, and this is shown in Fig. 4, with the control data from outside the light field plotted in Fig. 4(a) and the values from within the light field plotted in Fig. 4(b). In Fig. 4(a) there are no significant changes in the blood flow relative to the initial baseline value ( $P > 0.38$ ), whereas in Fig. 4(b) there was a significant decrease after all the six fractions, relative to the initial baseline value ( $P < 0.02$ ), based upon the Wilcoxon signed-ranks test.

Interestingly, while naturally occurring temporal oscillations in  $pO_2$  could be observed in some animals, there were also analogous oscillations in relative blood flow on the similar time scale of 40–60 s, as has been previously reported in this tumor model (29). The typical magnitude of oscillation would be near 10–20% of the total signal, yet not enough animals were studied to develop a statistical test of this.

### Blood pressure

In all rats included in this study the blood pressure remained above 70 mm Hg and was not significantly affected by the light treatment. In most rats there was a sudden jump in both  $pO_2$  and in blood pressure associated with the intravenous injection of the photosensitizer as might be expected. Other than this initial response there was minimal effect from the PDT as detected by blood pressure.

### Temperature measurement

Temperature measurements were taken both with and without BPD during irradiation in one rat tumor to determine the magnitude of heating caused by the light field with incident irradiance of  $200 \text{ mW/cm}^2$  at 690 nm. The maximal change *in vivo* was from  $35.2^\circ\text{C}$  resting to a peak of  $36.6^\circ\text{C}$  after 2 min of light irradiation. The temperature then tipped down to  $34.8^\circ\text{C}$  when the light was off. An irradiation for 4 min caused a rise from an initially  $34.1^\circ\text{C}$  up to  $36.0^\circ\text{C}$  in the same rat after it was injected with verteporfin. After the treatment the temperature then reduced to  $33.5^\circ\text{C}$  when the light was off.

### Photosensitizer extraction

The photosensitizer concentration as measured by fluorescence in the liquefied tissue was  $2.6 \pm 0.9 \text{ mg/kg}$  (mean  $\pm$  standard error of mean [SEM],  $n = 7$  animals), and the total range of variation was between 1.0 and  $3.7 \text{ mg/kg}$ .

## DISCUSSION

This study examines the effect of verteporfin photodynamic therapy on rat mammary tumor tissue oxygenation using microelectrodes that are able to sample regions of tissue that are smaller than the intercapillary distance. This method of sampling tissue is important because of the heterogeneous microregional oxygen distribution within dysplastic tissues. Verteporfin-based photodynamic therapy is currently being used for clinical treatment of the wet form of age-related macular degeneration. Also the potential use for dysplastic and tumor tissues is well documented in clinical (30) and preclinical studies (31–35). Although this photosensitizer elicits both direct cellular damage (36) as well as vascular occlusion, its main clinical use has been through the latter effect. Thus, assuming that the ability to cause vessel stasis is indicative of the successful treatment of tissue, it is possible to use the acute loss of  $pO_2$  as an endpoint to monitor treatment efficacy. To this end, we used spatially localized measurements in this study from each tumor to provide transient information about the response in a given region, and summarized all the measurements together to build up an illustration of how the tumor microheterogeneity would likely affect the treatment outcome within a single tumor. The implicit assumption in this experiment is that pooling localized data from several rats can provide a representative data set of the heterogeneity of responses within an individual animal's tissue.

Examination of the data presented in Figs. 1–3 indicates that the oxygen changes during treatment, and that the responses observed are highly heterogeneous between microregions of the tumor. The data in Figs. 2 and 3 indicate

that there is an overall acute reduction in  $pO_2$  during the course of the treatment. However, a drop is less likely to occur when the baseline  $pO_2$  is  $>8$  mm Hg. Oxygen tension dropped to near zero in many regions during the first light fraction, which mirrors the change in flow as measured during the same time interval. As can be seen from Fig. 1, there was a dose response in some cases where after two or three intervals the transient reoxygenation of the tissue ceased upon successive light-off fractions, thus indicative of a more permanent blood flow change such as vessel restriction or occlusion with higher total light doses. Interpretation of the blood flow changes requires care because the size of the Doppler probe used here was not as small as the oxygen electrode, and thus was not monitoring microregional responses, but rather a bulk tissue response. Also the Doppler probes could not be co-localized with the  $pO_2$  probes because of experimental limitations. However, in all cases, except one, where the flow was monitored in the treatment field the largest decrease in flow was observed after the first 2 min fraction of light.

The temperature changes monitored during the treatment of the tumor tissue were less than  $3^\circ$  with a maximum recorded *in vivo* temperature of  $36.6^\circ\text{C}$ . Mild temperature increases (near  $6^\circ\text{C}$ ) are well documented to cause increased tissue oxygen pressure, whereas the observed rise in the tumor temperature during PDT here was insufficient to cause this effect. Dewhirst *et al.* (37,38) have previously shown that in this tumor model these levels of temperature elevation would not induce significant  $pO_2$  change and are below the threshold of  $41^\circ\text{C}$  where significant changes might occur.

In summary, the  $pO_2$  data indicate that some highly oxygenated regions may not result in rapid occlusion of the type observed by Fingar *et al.* (6); however, their and other studies by Levy *et al.* (32) confirm that delayed onset of vascular occlusion can occur with verteporfin-based PDT. Independent of whether the effect is permanent or temporary, the observation of microregional dependence exists and indicates that the response to treatment is not homogeneous for all sites. The observation that oxygen decreases permanently in regions of initially low oxygenation indicates that there may be no oxygen limitation to this PDT-induced vascular occlusion process; however, it is difficult to validate this without further experiments that examine the vessels flow directly. Based upon the data from the areas of initially high  $pO_2$ , we can conclude that there is not always acute vessel occlusion from the treatment used here, and that these areas are likely in regions of vessels with good perfusion. In the case of areas with initially low  $pO_2$ , it is not directly known if these regions are areas of low flow or simply just distant from any vessels that have high flow; however, the response to treatment is clearly different than in the high- $pO_2$  areas. Thus, if the response in areas of low  $pO_2$  is uniform, it appears unlikely that this can be explained as areas that are simply distant from high-flowing vessels. It appears more likely that these regions of initially low  $pO_2$  are near vessels that have a low flow rate and are more readily occluded by the treatment; however, further experiments need to be completed to confirm this. The implications of this conclusion are significant, for if regions of high  $pO_2$  appear to be resistant to PDT-induced vessel stasis, then these regions may be the areas that result in lesion regrowth caused by insufficient

treatment. This suggests that dosimetry strategies need to be developed to preferentially target the high-flow vessels for effective treatment in this type of PDT. However, it is important to determine if the lack of vessel occlusion observed here is representative of the longer-term response (over hours and days) rather than simply a difference in the immediate vessel occlusion response.

Further analysis is needed to examine what conditions maximize the occlusion selectivity of neovasculature *versus* normal vessels, and what the characteristic temporal responses for occlusion are in different vessels. Further study is needed using colocalized measurements of oxygen and blood flow, perhaps using a tumor window chamber type experiment, where the two measurements can be directly observed spatially. A comparison of tumor microvasculature relative to normal or peri-tumor regions could provide information about the selectivity of the treatment for specific lesions (6), and similarly an analysis of the mechanisms of vessel stasis relative to the flow velocity would provide information about methods to improve overall treatment efficacy. The type of microscopic dosimetry evaluation used here is essential to provide a mechanistic understanding of the heterogeneity of response in photodynamic therapy treatment within individual tissue types.

*Acknowledgements*—The authors would like to thank Dr. Julia A. O'Hara for the use of her spectrofluorimeter and Drs. H. M. Swartz, J. A. O'Hara, P. J. Hoopes, T. Hasan and B. C. Wilson for their thoughtful discussions about this study. This work has been supported by NIH grant RO1CA78734 (B.W.P.), and the photosensitizer has been supplied by QLT Phototherapeutics, Inc. (Vancouver, BC, Canada).

## REFERENCES

1. Dougherty, T. J., C. J. Gomer, B. W. Henderson, G. Jori, D. Kessel, M. Korbelik, J. Moan and Q. Peng (1998) Photodynamic therapy. *J. Natl. Cancer Inst.* **90**(12), 889–905.
2. Levy, J. G. (1994) Photosensitizers in photodynamic therapy. *Semin. Oncol.* **21**(6) (Suppl. 15), 4–10.
3. Levy, J. G. (1999) Photodynamic therapy of subfoveal choroidal neovascularization in age-related macular degeneration with verteporfin: one-year results of 2 randomized clinical trials—TAP report. Treatment of age-related macular degeneration with photodynamic therapy (TAP) study group. *Arch. Ophthalmol.* **117**(10), 1329–1345.
4. Schmidt-Erfurth, U., J. W. Miller, M. Sickenberg, H. Laqua, I. Barbazetto, E. S. Gragoudas, L. Zografos, B. Piguat, C. J. Pournaras, G. Donati, A. M. Lane, R. Birngruber, H. van den Berg, H. A. Strong, U. Manjuri, T. Gray, M. Fsadni and N. M. Bresler (1999) Photodynamic therapy with verteporfin for choroidal neovascularization caused by age-related macular degeneration: results of retreatments in a phase 1 and 2 study. *Arch. Ophthalmol.* **117**(9), 1177–1187.
5. Fong, D. S. (2000) Age-related macular degeneration: update for primary care. *Am. Fam. Phys.* **61**(10), 3035.
6. Fingar, V. H., P. K. Kik, P. S. Haydon, P. B. Cerrito, M. Tseng, E. Abang and T. J. Wieman (1999) Analysis of acute vascular damage after photodynamic therapy using benzoporphyrin derivative (BPD). *Br. J. Cancer* **79**(11–12), 1702–1708.
7. Fenton, B. M., E. K. Rofstad, F. L. Degner and R. M. Sutherland (1988) Cryospectrophotometric determination of tumor intravascular oxyhemoglobin saturations: dependence on vascular geometry and tumor growth. *J. Natl. Cancer Inst.* **80**(20), 1612–1619.
8. Dewhirst, M. W., E. T. Ong, B. Klitzman, T. W. Secomb, R. Z. Vinuya, R. Dodge, D. Brizel and J. F. Gross (1992) Perivascular oxygen tensions in a transplantable mammary tumor growth

- ing in a dorsal flap window chamber. *Radiat. Res.* **130**(2), 171–182.
9. Fenton, B. M. and B. A. Way (1993) Vascular morphometry of KHT and RIF-1 murine sarcomas. *Radiother. Oncol.* **28**, 57–62.
  10. Fenton, B. M. and D. W. Siemann (1994) Investigations of perfusion-limited hypoxia and oxygenation in the KHT sarcoma. *Adv. Exp. Med. Biol.* **361**, 627–634.
  11. Dewhirst, M. W., E. T. Ong, G. L. Rosner, S. W. Rehmus, S. Shan, R. D. Braun, D. M. Brizel and T. W. Secomb (1996) Arteriolar oxygenation in tumour and subcutaneous arterioles: effects of inspired air oxygen content. *Br. J. Cancer* **27**, S241–S246.
  12. Dewhirst, M. W., H. Kimura, S. W. Rehmus, R. D. Braun, D. Papahadjopoulos, K. Hong and T. W. Secomb (1996) Microvascular studies on the origins of perfusion-limited hypoxia. *Br. J. Cancer* **27**, S247–S251.
  13. Helmlinger, G., F. Yuan, M. Dellian and R. K. Jain (1997) Interstitial pH and pO<sub>2</sub> gradients in solid tumors *in vivo*: high-resolution measurements reveal a lack of correlation. *Nat. Med.* **3**(2), 177–182.
  14. Dewhirst, M. W., E. T. Ong, R. D. Braun, B. Smith, B. Klitzman, S. M. Evans and D. Wilson (1999) Quantification of longitudinal tissue pO<sub>2</sub> gradients in window chamber tumours: impact on tumour hypoxia. *Br. J. Cancer* **79**(11–12), 1717–1722.
  15. Tromberg, B. J., A. Orenstein, S. Kimel, S. J. Barker, J. Hyatt, J. S. Nelson and M. W. Berns (1990) *In vivo* tumor oxygen tension measurements for the evaluation of the efficiency of photodynamic therapy. *Photochem. Photobiol.* **52**(2), 375–385.
  16. Foster, T. H., D. F. Hartley, M. G. Nichols and R. Hilf (1993) Fluence rate effects in photodynamic therapy of multicell tumor spheroids. *Cancer Res.* **53**(6), 1249–1254.
  17. Nichols, M. G. and T. H. Foster (1994) Oxygen diffusion and reaction kinetics in the photodynamic therapy of multicell tumour spheroids. *Phys. Med. Biol.* **39**, 2161–2181.
  18. Georgakoudi, I., M. G. Nichols and T. H. Foster (1997) The mechanism of Photofrin photobleaching and its consequences for photodynamic dosimetry. *Photochem. Photobiol.* **65**(1), 135–144.
  19. Sitnik, T. M., J. A. Hampton and B. W. Henderson (1998) Photodynamic therapy reduces tumor oxygenation during and after treatment: effects of fluence rate. *Br. J. Cancer* **77**(9), 1386–1394.
  20. Henderson, B., T. M. Busch, L. A. Vaughan, N. P. Frawley, D. Babich, T. A. Sosa, J. Zollo, A. Dee, M. Cooper, D. Bellnier, W. Greco and A. Oseroff (2000) Photofrin photodynamic therapy can significantly deplete or preserve oxygenation in human basal cell carcinomas during treatment, depending on fluence rate. *Cancer Res.* **60**, 525–529.
  21. Star, W. M., H. P. Marijnissen, A. E. van den Berg-Blok, J. A. Versteeg, K. A. Franken and H. S. Reinhold (1986) Destruction of rat mammary tumor and normal tissue microcirculation by hematoporphyrin derivative photoradiation observed *in vivo* in sandwich observation chambers. *Cancer Res.* **46**(5), 2532–2540.
  22. Wieman, T. J., T. S. Mang, V. H. Fingar, T. G. Hill, M. W. Reed, T. S. Corey, V. Q. Nguyen and E. R. Render Jr. (1988) Effect of photodynamic therapy on blood flow in normal and tumor vessels. *Surgery* **104**(3), 512–517.
  23. Fingar, V. H., T. J. Wieman, S. A. Wiehle and P. B. Cerrito (1992) The role of microvascular damage in photodynamic therapy: the effect of treatment on vessel constriction, permeability, and leukocyte adhesion. *Cancer Res.* **52**(18), 4914–4921.
  24. Pogue, B. W., J. A. O'Hara, K. J. Liu, T. Hasan and H. M. Swartz (1999) Photodynamic treatment of the RIF-1 tumor with verteporfin with online monitoring of tissue oxygen using electron paramagnetic resonance oximetry. *Proc. SPIE: Laser Tissue Interact. X* **3601**, 108–114.
  25. Whalen, W., J. Riley and P. Nair (1967) A microelectrode for measuring intracellular pO<sub>2</sub>. *J. Appl. Physiol.* **23**, 798–801.
  26. Schneiderman, G. and T. Goldstick (1978) Oxygen electrode design criteria and performance characteristics: recessed cathode. *J. Appl. Physiol. Respir. Environ. Exerc. Physiol.* **45**, 145–154.
  27. Dewhirst, M. W., T. W. Secomb, E. T. Ong, R. Hsu and J. F. Gross (1994) Determination of local oxygen consumption rates in tumors. *Cancer Res.* **54**(13), 3333–3336.
  28. Linsenmeier, R. A. and C. M. Yancey (1987) Improved fabrication of double-barreled recessed cathode O<sub>2</sub> microelectrodes. *J. Appl. Physiol.* **63**, 2554–2557.
  29. Braun, R. D., J. L. Lanzen and M. W. Dewhirst (1999) Fourier analysis of fluctuations of oxygen tension and blood flow in R3230Ac tumors and muscle in rats. *Am. J. Physiol.* **277**(2 Pt. 2), H551–568.
  30. Lui, H., L. Hruza, D. McLean, N. Kollias, J. Wimberly, M. Gagel, V. Salvatori and R. Anderson (1994) Photodynamic therapy of malignant skin tumors in humans with Benzoporphyrin derivative and 690-nm laser-light. *J. Invest. Dermatol.* **102**(4), 569–569.
  31. Hsiang, Y. N., M. T. Crespo, A. M. Richter, A. K. Jain, M. Frago and J. G. Levy (1993) *In vitro* and *in vivo* uptake of benzoporphyrin derivative into human and miniswine atherosclerotic plaque. *Photochem. Photobiol.* **57**(4), 670–674.
  32. Levy, J. A., E. Waterfield, A. Richter, S. C., H. Lui, H. L., A. R. and V. Salvatori (1993) Photodynamic therapy of malignancies with benzoporphyrin derivative monoacid ring A. *Proc. SPIE* **2078**, 91–98.
  33. Wyss, P., Y. Tadir, B. J. Tromberg, L. Liaw, T. Krasieva and M. W. Berns (1994) Benzoporphyrin derivative—a potent photosensitizer for photodynamic destruction of rabbit endometrium. *Obstet. Gynecol.* **84**(3), 409–414.
  34. Molpus, K. L., D. Kato, M. R. Hamblin, L. Lilge, M. Bamberg and T. Hasan (1996) Intraperitoneal photodynamic therapy of human epithelial ovarian carcinomatosis in a xenograft murine model. *Cancer Res.* **56**, 1075–1082.
  35. Momma, T., M. R. Hamblin, H. C. Wu and T. Hasan (1998) Photodynamic therapy of orthotopic prostate cancer with benzoporphyrin derivative: local control and distant metastases. *Cancer Res.* **58**, 5425–5431.
  36. Iinuma, S., K. T. Schomacker, G. Wagnieres, M. Rajadhyaksha, M. Bamberg, T. Momma and T. Hasan (1999) *In vivo* fluence rate and fractionation effects on tumor response and photobleaching: photodynamic therapy with two photosensitizers in an orthotopic rat tumor model. *Cancer Res.* **59**(24), 6164–6170.
  37. Dewhirst, M. W., J. F. Gross, D. Sim, P. Arnold and D. Boyer (1984) The effect of rate of heating and cooling prior to heating on tumor and normal tissue microcirculatory blood flow. *Biorheology* **21**, 539–558.
  38. Dewhirst, M. W., D. A. Sim, J. F. Gross and M. A. Kundrat (1986) Effects of heating rate on normal and tumor microcirculatory function. In *Heat and Mass Transfer in the Microcirculation of Thermally Significant Vessels* (Edited by R. B. R. K. R. Diller), pp. 75–80. ASME, New York.